RSC Advances

ROYAL SOCIETY OF CHEMISTRY

www.rsc.org/advances

Electrospun nanofibrous composites of polystyrene and cellulose nanocrystals: manufacture and characterization

Siqi Huan, Long Bai, Guangping Han*

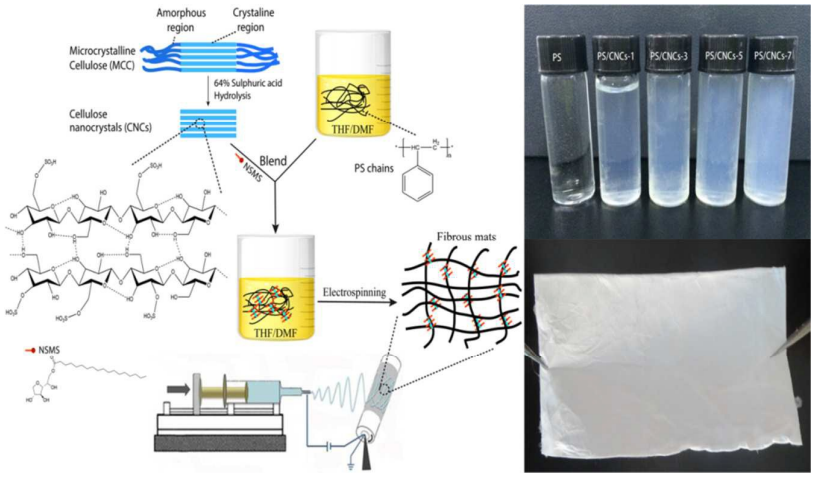

Electrospun nanofibrous composites of polystyrene and cellulose nanocrystals: manufacture and characterization

Siqi Huan, Long Bai, Guoxiang Liu, Guangping Han*

College of Material Science and Engineering, Northeast Forestry University, Harbin 150040, PR China

Corresponding author: Guangping Han; **E-mail address:** guangping.han@nefu.edu.cn; **Tel:** +86-15046691858

Abstract: An electrospinning process was successfully utilized to manufacture polystyrene/cellulose nanocrystal (PS/CNC) nanofibrous mats. Morphology, crystallinity, thermal behavior, as well as mechanical and hydrophobic properties of electrospun PS/CNC nanofibrous mats were investigated. Morphological analysis of the obtained nanofibrous mats demonstrated that fine nanofibers with smooth and smaller diameter could be obtained with increased CNC contents. Fourier transform infrared spectroscopy (FTIR) and X-ray photoelectron spectroscopy (XPS) results showed that PS and CNCs were physically mixed and CNCs were probably distributed on the surface of the electrospun nanofibers. The structural property e.g. crystallinity of the electrospun nanofibers was examined using wide angle X-ray diffraction (WAXD). It was indicated that crystallinity could be increased as a result of the increased addition of CNCs and aligned nanofiber orientation. Thermal properties of electrospun PS/CNC nanocomposites were enhanced by increasing CNC loading levels. The tensile strength of electrospun PS/CNC nanofibrous mats was elevated 170% by incorporating 7 wt% CNCs in PS matrix, while the ductility was decreased from 60 to 25%. The hydrophobic property could be increased to 138° when 1 wt% CNCs was incorporated.

Keywords: electrospinning technique; cellulose nanocrystals; polystyrene; nanofibrous mat

1 Introduction

Nanomaterials based on renewable resources are attracting rapidly growing interest from the perspective of developing novel structural and functional heterogeneous materials that occur at the nanometer length scale [1]. Cellulose that consists of crystalline and amorphous regions is one of the most versatile and abundant renewable resources for nature-based materials [2-4]. One recent strong trend is focused on the isolation of cellulose with diameters in the nanometer range and to utilize their dimensional effect to develop novel cellulose-based materials with diverse advanced functionalities [5]. Significant advances in the preparation of cellulose nanocrystals (CNCs) have been made using a number of procedures, including acid hydrolysis [6], mechanical isolation [7], and ultrasonication [8], etc. Among them, acid hydrolysis to produce CNCs is a simple, well-developed technique allowing precise control over the CNC's physical and chemical characteristics [9]. CNC features an attractive combination of properties such as biocompatibility, biodegradability, high mechanical strength, and flexible surface chemistry, making it of interest in applications such as composites [10], modular building block [11] and hydrogels [12]. Particularly, CNC is one of the optimal candidates for tailoring mechanical properties of polymer materials due to its densely and orderly crystallized structure after acid hydrolysis [13]. However, full utilization of the intrinsic properties of CNCs requires the development of robust and versatile synthetic and processing routes to afford controllable nanocomposite.

Polystyrene (PS) is a class of low coat, promising thermoplastic polymers. The inherent hydrophobicity of PS has been extensively explored and utilized to create superhydrophobic materials with tailed performances [14]. Nevertheless, its brittleness and poor heat mechanical properties make its application limited. Great effort has been made through various approaches to improve the shortcomings of PS materials, including blending [15], fabricating novel architecture [16], and new processing technique [17], etc. In recent years, numerous publications have been highlighted on the improved properties of modified PS materials [18-19]. However, such approaches either are limited to create PS materials with specific components, or need complex fabricating process. In fact, no simple PS modified formulation is commercially available that can offer potential to concurrently overcome all the drawbacks of PS materials and improve the inherent hydrophobic advantage. Therefore, the development of simple, synergistic methods to prepare high-performance PS-based materials is critical.

CNC potentially has great utility as composite building block to enhance the properties of PS materials. However, one disadvantage of CNC in term of its reinforcement in hydrophobic PS materials is its strong hydrophilicity resulted from large amount of surface hydroxyl [20], leading to aggregation or nonhomogeneous dispersion of CNCs into nonpolar PS

continuous matrix. It has been well known that homogeneous dispersion of CNCs in the polymer matrix is an important prerequisite to benefit from its dimensional effect and other superior properties [21]. The major issue that limits the elegant blending of PS and CNCs is the inherent incompatibility resulted from large differences of polarity between these constituents. Furthermore, CNCs have great trend to self-aggregation in continuous phase due to its nanoscale and large surface area. One effective way to homogeneously disperse CNCs and to enhance interfacial compatibility with nonpolar PS is adding amphipathic surfactant [22]. However, although PS and CNCs can be well blended after adding proper surfactant, the properties of PS/CNC nanocomposite materials prepared by conventional processing method may still decrease because the dynamically phase separation can be induced by external stimuli during preparation (e.g. temperature and evaporation rate). Electrospinning technique provides an alternative way to fabricate PS/CNC nanocomposite by using the blending of PS and CNCs. The simplicity and rapidity of electrospinning process is beneficial for fabricating PS/CNC nanocomposite because phase reconfiguration can be blocked under rapid preparation process, leading to a homogeneous enhancement of CNCs in PS matrix. Electrospinning is also a powerful tool to create high-performance and multi-functional materials by tuning the surface structure of nanofibrous mats [23-24], providing a variety of fascinating characteristics such as small fiber diameters, ordered morphology and an interconnected network desirable for a range of applications [25-26]. However, because of the hydrophilic nature of CNCs, a number of publications have been only focused on the electrospinning process of water-soluble polymer/CNC nanocomposite, including poly(lactic acid)/CNCs [27], poly(vinyl alcohol)/CNCs [28], and poly(ethylene oxide)/CNCs [29], and few studies have attempted to produce hydrophobic polymer/CNCs nanocomposite, especially PS/CNCs [30]. Furthermore, the composite morphologies and structure-property relationships of electrospun hydrophobic polymer/CNC nanocomposite have not yet been fully explored. Herein, taking advantages of the characteristics of constituents and electrospinning process, PS-based fibrous nanocomposite with modified inherent shortcomings and improved hydrophobicity was successfully manufactured by electrospinning hydrophobic PS/hydrophilic CNCs blends, and a mechanism to control the hydrophilic-hydrophobic property of nanofibrous mats was proposed. To our knowledge, this is the first report related to controllably increasing the hydrophobicity of PS-based nanomaterials through incorporating hydrophilic CNCs.

In this work, a series of PS/CNC composite nanofibrous mats with different CNC contents were fabricated by electrospinning process (Fig.1). The CNCs were isolated from acid hydrolysis of microcrystalline cellulose (MCC). The blending of PS and CNCs was promoted by adding proper surfactant. The main objective of this research is to utilize a simple synergistic approach, through blending and electrospinning process, to incorporate hydrophilic modified component CNCs into hydrophobic PS matrix, manufacturing high-performance PS/CNC nanocomposite, especially in the aspect of superhydrophobic PS-based nanomaterials. The effect of CNC contents on the morphologies, compositions and nanofiber surface properties of the electrospun PS/CNC nanocomposite was evaluated and discussed. Evaluations of PS/CNC nanocomposite performances, e.g. mechanical property and hydrophobic property, were undertaken to investigate the structure-property relationship.

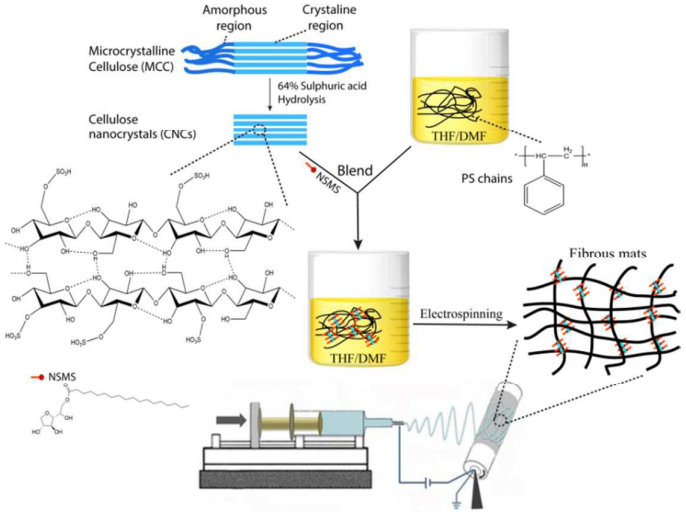

Fig.1. Manufacture process of the electrospun PS/CNC composite nanofibrous mats

2 Experimental

2.1 Materials

Polystyrene (PS) particles (M_w=260,000), sulfuric acid (98 wt%), and nonionic sorbitan monostearate (NSM) as surfactant were purchased from Aladdin (Shanghai, China). Microcrystalline cellulose (KY100S MCC, moisture content=75%, Daicel Co., Japan) was used as the raw material for producing CNCs. *N,N*-dimethylformamide (DMF) and Tetrahydrofuran (THF) (AR grade, Kermel Co., Tianjin, China) were of analytical grade and used as received without further purification. Deionized water was used throughout the study.

2.2 Preparation of cellulose nanocrystals

Forty grams of MCC were mixed with 170 mL of 64 wt% sulfuric acid aqueous solution, and the mixture was stirred vigorously at 45℃ for 1h. CNCs were isolated from the obtained mixture by combined centrifugation and dialysis as reported in the previous paper [6]. After dialysis, the yield was calculated by withdrawing a known, small amount of the sample and obtaining its oven-dried weight. The pelleted CNCs obtained after dialysis were dried using a freeze dryer (Scientz-10N, Xin Zhi Co., China).

2.3 Preparation of spinning solution

One typical process for preparing spinning solution in this work is described as below. PS particles were dissolved in the mixture of DMF and THF at the ratio of 3:1 under vigorous magnetic stirring at room temperature for 12 h to obtain a 20 wt% concentrated PS solution. The pelleted CNCs obtained as described above and NSM (1% PS weight) were added into PS solution and agitated for 12 h before electrospinning. The CNC loading percentage in relation to the adding weight of PS was chosen as 0, 1, 3, 5, 7%. The samples were designed as PS/CNC-x, where x (wt%) is CNC loading level.

2.4 Electrospinning set-up

The electrospinning apparatus (Yong Kang Le Ye Co., Beijing, China) with a 5mL syringe (Zhi Yu Co., Shanghai, China) connected to a syringe pump that was encased in a vented Plexiglas box [950 mm (L) × 820 mm (W) × 950 mm (H)]. The syringe pump was used to supply a steady flow of 0.0625 $ml \cdot min^{-1}$ of solution to the tip of the needle. A high-voltage power supply was used to apply a potential to the syringe needle. The needle used was size 22 and the corresponding inner diameter was 0.4mm. The target with a grounded cylinder collector (340 mm in length and 108 mm in diameter) was rotated at a speed of 80 rpm and placed certain distance from the needle tip to test the distances that the fibers were dry upon collection. A rectangular piece of aluminum foil (240 mm in length and 150 mm in width) was covered on the cylinder to collect nonwovens of the electrospun nanofibers. The relative humidity and temperature were constantly monitored at 13% and 25℃, respectively, by a hygrothermograph placed inside of the electrospinning chamber.

2.5 Characterization of spinning solution

Conductivity, viscosity, and surface tension of the PS/CNC solutions were characterized at room temperature using a conductivity meter (DDSJ-318, Lei Ci Co., Shanghai, China), digital rotational viscometer (SNB-1, Heng Ping Co., Shanghai, China), and a surface tension meter (JK99B, Zhong Chen Co., Shanghai, China), respectively.

The morphologies of the obtained CNCs and spinning solutions were observed using a transmission electron microscopy (TEM, Hitachi-7650, Japan). For the analysis, aqueous CNC suspensions and prepared spinning solutions were all diluted to 0.05 to 0.1 wt%. A droplet of diluted suspension was negatively stained with 5 μL of 2 wt % uranyl acetate for about 2 min to enhance the contrast of the TEM images. The mixture was then immediately deposited on the surface of a 400-mesh carbon-coated copper grid, and then was observed under an accelerating voltage of 80 kV. The particle dimensions were calculated from the TEM images using Nanometer software (Fu Dan University, China). For each sample, one hundred particles were randomly selected and measured from several TEM images.

2.6 Evaluation of electrospun nanofibrous mats

Scanning electron microscope (SEM, QUANTA-200, FEI, Hillsboro, OR, United States) was used to obtain microphotographs of the non-woven nanofibers formed after electrospun. The nanofibrous mats were collected on the aluminum foils. The mats were cut into pieces, and then coated with a layer of gold-palladium before being observed with the SEM at an accelerating voltage of 12.5 kV. The diameter and distribution of the electrospun nanofibers were analyzed from the SEM images by Nanometer software (Fu Dan University, China). At least 100 nanofibers were measured to obtain the average fiber diameter.

Fourier transform infrared spectroscopy (FTIR, NICOLET 6700, Thermo Fisher Scientific, Agawam, MA, United States) was used to obtain the spectra of each sample to examine any changes in the chemical structure of the electrospun PS/CNC nanocomposite. Each spectrum was acquired in a transmittance mode on a Zn/Se ATR crystal cell by accumulation of 64 scans with a resolution of 4 cm^{-1} and a spectral range of 4000-500 cm^{-1}. Spectral outputs were recorded as a function of wavenumber.

The surface composition of the electrospun PS/CNC nanofibrous mats were detected by X-ray photo electron spectroscopy (XPS, K-Alpha, Thermo Fisher Scientific, Agawam, MA, United States) using a PHI5700 spectrometer and Al Kσ radiation (hυ=1486.6 eV). Binding energies were referenced to the O_{1s} line at 201 eV. Quantitative analysis of oxygen was obtained from the peak intensities of the O_{1s} signals.

Wide-angle x-ray diffraction (WXRD, D/MAX 2200, Rigaku, Japan) data were generated by a diffractometer with Cu Kα radiation (λ=1.542Å) at 40 kV and 30 mA over the angular range 2θ= 5°-40°, a step size of 4°·min^{-1}. The degree of crystallinity or crystallinity index (CI, %) for CNC and PS/CNCs was evaluated using Equation (1).

$$\mathrm{CI} = {}^{A_c}/_{A_a} \times 100\% \quad (1)$$

where A_c is the area of the crystalline reflection and A_a is the area subtending the whole diffraction profile.

Differential Scanning Calorimetry (DSC) measurements were performed with a Netzsch (DSC-204, Germany) instrument at 5℃·min^{-1} heating rate from room temperature to 160℃ in a 50 mL·min^{-1} dynamic N_2 atmosphere. Samples of about 5 mg were loaded into DSC pans sealed using a crimping tool. The T_g of the sample was defined as the midpoint temperature of glass transition. All tests were carried out in duplicate.

Thermogravimetric analysis (TGA, TGA-209, Netzsch, Germany) was conducted to study thermal decomposition of electrospun PS/CNC nanofibrous mats. Samples of 5-10 mg were heated from room temperature to 700℃ at a rate of 5℃·min^{-1} under Ar atmosphere. The onset decomposition temperature and the maximum thermal decomposition temperature of samples were defined as T_{onset} and T_{max}, respectively.

Mechanical properties of the electrospun PS/CNC composite nanofibrous mats were determined from the stress-strain curves from tensile test. The tensile test of the samples was carried out on a Model 3365 universal testing machine (Instron Co., Norwood, MA, United States) with a tensile rate of 10 mm·min^{-1} according to the ASTM D 882-09 at room temperature and 30% humidity. The size of each sample was 15 mm length and 5 mm width. Three replications of the mats prepared at each composition were measured.

The wettability of the electrospun PS/CNC nanofibrous mat surface was recorded on a contact angle meter (OCA20, Dataphysics, Bad Vilbel, Germany) at ambient. Contact Angle (CA) was measured using a sessile drop method. A droplet of 5 μL volume was used. The CA values of the right side and the left side of the water droplet were both measured and averaged. All the CA data were an average of five measurements on different locations of the surface.

3 Results and Discussion

3.1 Properties of spinning solution

Fig.2 displays the TEM images of isolated CNCs and prepared spinning solution of PS/CNC-7. In Fig.2(a), it reveals that homogenized CNCs after treatment with 64 wt % H_2SO_4 were well isolated. The size and shape of the obtained CNCs were finely controlled and exhibited a rod-shape structure with a width of 9 ± 3 nm and a length of 138 ± 28 nm, respectively. The corresponding aspect ratio of the obtained CNCs was 13.8 to 15.3. Fig.2(b) shows that in spinning solution, PS chains were assembled as spherical particles with uniform size, and CNCs were homogeneously dispersed around PS particles. As shown in Fig.1, amphipathic surfactant, NSM, was used to enhance the dispersity of CNCs within spinning solvent in the presence of PS, and to reduce the self-aggregation of CNCs in the PS solution. It is attributed that the hydrophilic end-groups of NSM can interact with the surface -OH of CNCs, and the hydrophobic alkane chains can stretch into solvent phase, adsorb with PS chains, and then form a water-in-oil colloidal system, affording sufficient stability for CNCs dispersion. Fig.3 shows the photograph of prepared spinning solutions with different CNC contents. It can also be seen that pure PS solution was colorless and transparent, while the stable spinning solutions with various CNC contents turned to be increasingly turbid with increasing CNC loadings. Table 1 shows the viscosity, surface tension, and conductivity data of pure PS solution and PS/CNC suspensions. The surface tension of PS/CNC suspensions decreased

slightly compared with that of PS solutions. The conductivity significantly increased with increasing CNC contents attributing to the presence of high surface sulfate ester groups of CNCs obtained from the sulfuric acid hydrolysis during CNCs production [31]. The increased viscosity for PS/CNC suspensions was observed with the increase of CNC contents likely because of the addition of NSM. The polar CNCs and the nonpolar PS may form connected network structure within the polymer solutions due to the function of NSM [22]. Furthermore, the association of surface -SO_3H ionic groups may also increase the viscosity.

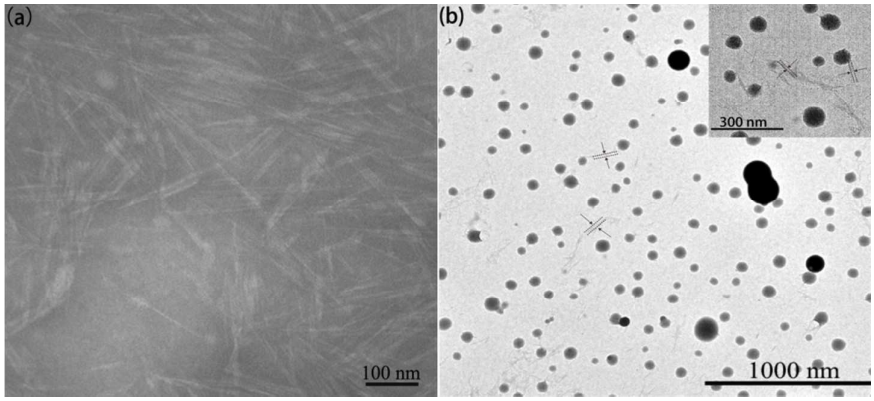

Fig.2. TEM images of (a) manufactured cellulose nanocrystals and (b) spinning solution of PS/CNC-7. The inset image in (b) represents the magnified TEM image of spinning solution.

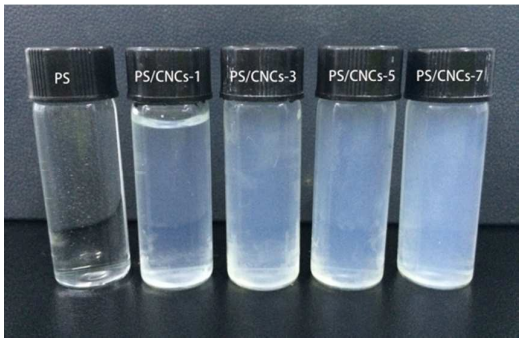

Fig.3. Photograph of spinning solutions with various CNC contents

Table 1 Characteristic properties of tested solutions[a]

Code	Viscosity (mPa·s)	Surface tension (mN/m)	Conductivity (F/m)
PS	321±5	33.924±2	0.295±0.01
PS/CNC-1	346±3	33.833±3	2.79±0.2
PS/CNC-3	368±7	33.752±2	4.58±0.3
PS/CNC-5	395±6	33.293±2	5.32±0.9
PS/CNC-7	412±8	33.078±3	7.95±1.1

[a] Data are given as the mean value ± standard deviation..

3.2 Morphology of Nanofibrous Mats

SEM images of electrospun PS and PS/CNC nanofibers with different CNC contents are presented in Fig.4. The SEM images and diameters of electrospun PS/CNC nanofibers with adding 7 wt% CNC produced from various electrospinning parameters were documented in **Supporting Information** (Figure S1 to Figure S4). From Fig.4, it is displayed that all produced nanofibers exhibited uniform diameters without visible bead or bead-to-string structure. Fig.4(a) shows that the surface morphology of electrospun pure PS nanofibers was rougher than those of electrospun PS/CNC nanofibers. With the increased addition of CNCs, the surface structure of electrospun nanofibers gradually turned to be smooth as shown from Fig.4(b) to (e). The calculated average nanofiber diameters and diameter deviations of electrospun nanofibers are displayed in Fig.4(f). The average diameter of electrospun PS nanofiber was about 2.23 μm. When adding 1 wt% CNC, the fiber diameter was greatly increased to 3.5 μm. With further increasing CNC loading levels, however, the fiber diameters could

significantly decrease to 2.31, 2.23, and 2.33 μm, which were comparable with that of electrospun PS. It has been demonstrated that the variations of viscosity, surface tension and conductivity of spinning solutions played decisive roles in determining the structure and diameter of electrospun nanofibers [32]. The increment of conductivity often results in production of uniform bead-free and smaller nanofiber diameter since the polymer jet is subjected to more stretching under the high electrical field. The surface tension can afford counterforce to resist the electrostatic force which is useful to form greater elongation, however, the excessive surface tension can make the polymer jets into spheres for decreasing the surface area per unit mass. Furthermore, the increase of viscosity also preferred to fabricating fibers featuring uniform diameters and surface structure because high viscosity can reduce the rapid shape transformation of polymer jets. As shown in Table 1, the viscosity and conductivity of spinning solution both significantly increased with increasing the amount of CNCs while surface tension slightly decreased. Therefore, with increased addition of CNCs, the markedly increased electrostatic force resulted from larger conductivity could easily overcome the proper surface tension of polymer solutions to stretch PS/CNC polymer jets to a greater extent during electrospinning process. Meanwhile, the high viscosity of PS/CNC solution could provide sufficient resistance to reduce rapid shape transformation and recovery, leading to a steady electrospinning process with smooth fiber surface. Taken together, the fine PS/CNC nanofibers with smooth surface and uniform diameter can be controllably produced by electrospinning polymer solutions with various CNC contents.

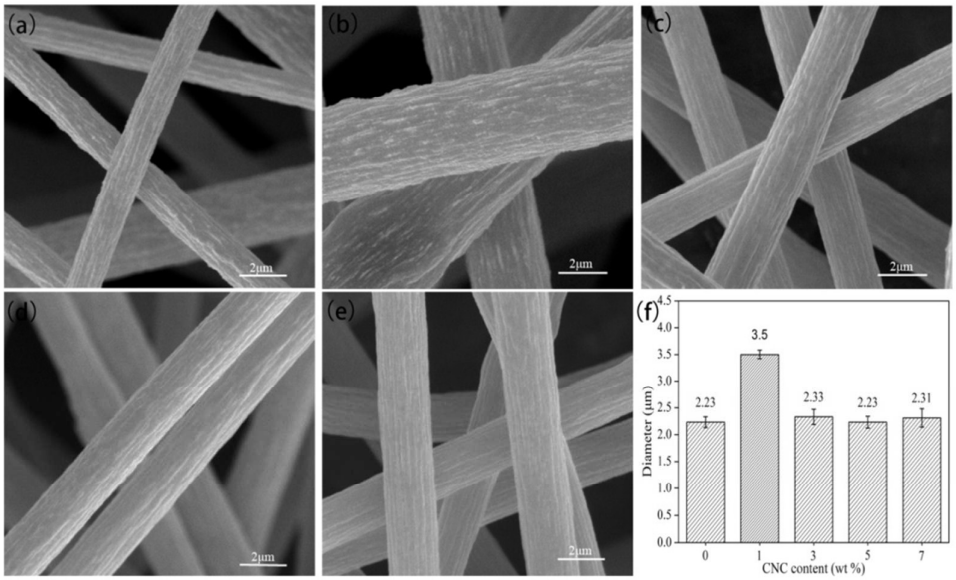

Fig.4. SEM images of electrospun nanofibrous mats with different CNC contents when electrospinning voltage was 15kV, solution concentration was 20 wt%, and the ratio of DMF to THF was 3:1.(a) PS (b) PS/CNC-1 (c) PS/CNC-3 (d) PS/CNC-5 (e) PS/CNC-7 (f) Average diameters of different nanofibers

3.3 Surface Characteristics of Nanofibrous Mats

FTIR spectra of the electrospun nanofibrous mats and CNC powders are presented in Fig.5(a). For original CNC powders, the absorbance peaks in the range 3600-3200 cm^{-1} are attributed to the stretching of the -OH groups of cellulose, and the peaks around 2900-2800 cm^{-1} correspond to C-H stretching. The peaks observed at 1426 and 1315 cm^{-1} in the spectrum of the CNCs are attributed to the symmetric bending of $-CH_2$ and the bending vibrations of the C-H and C-O groups of the rings in polysaccharides, respectively [34]. The stretching vibration at 1033 cm^{-1} was attributed to C-O at C-6 of CNCs. Pure PS shows three obvious characteristic absorption bands. The lower absorbance intensities at 3200-2800 cm^{-1} were assigned as C-H symmetric and asymmetric vibration, the wavenumber at 1600-1400 cm^{-1} corresponds to the bending vibration and the stronger intensities around 770-650 cm^{-1} attributes to the mono-substituted benzene. As increased addition of CNCs, the characteristic bands of PS were strengthened because of overlapping of absorbance peaks of CNCs and PS. Furthermore, the appeared new peak at 1033 cm^{-1} attributed to C-O of CNCs was also strengthened. The -OH group peak of CNCs was almost disappeared due to the small amount of CNCs comparing with PS. The differences between CNCs, PS, and PS/CNC-1, 3, 5, 7 clearly showed that electrospun nanofibers consisted of PS and CNCs initially presented in the polymer solution (i.e., no component was selectively excluded during electrospinning). It is also indicated that the PS

particles, CNCs and NSM were physically blended, and there were no chemical reaction happened and no chemical bond formed during electrospinning process.

Fig.5(b) shows the O_{1s} XPS spectra of the electrospun nanofibrous mats. From Fig.5(b), three kinds of chemical state of oxygen, C-O (existed in CNCs), C=O (both in CNCs and NSM), and absorbed oxygen (originated from air), were observed. It is considered that the spectrum of absorbed oxygen was responsible for the observed oxygen in PS. More importantly, it is shown that there indeed existed CNCs and NSM on the surface of nanofibers, demonstrating the proposed nanofibrous mat structure in Fig.1. The variation of oxygen content (at%) is listed in Table 2 to further illustrate the quantitative characteristics of surface CNCs and NSM. It is apparent that the surface oxygen content was significantly increased with increasing the addition of CNCs amount, providing direct evidence for the existence of surface CNCs.

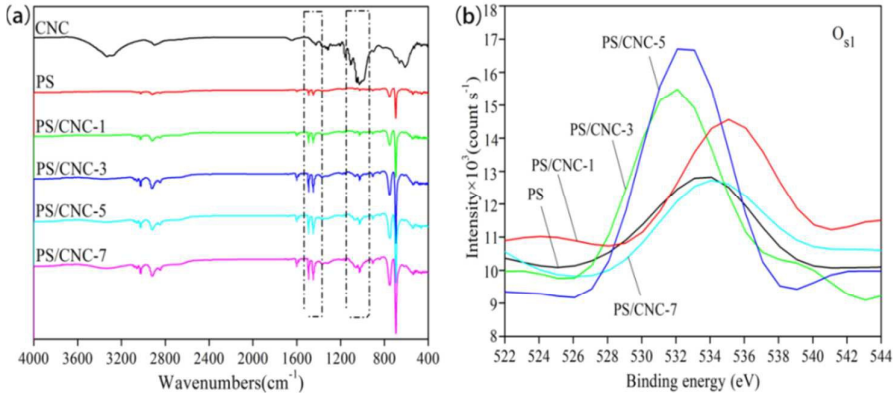

Fig.5. (a) FTIR spectra of CNCs and electrospun PS/CNC nanofibrous mats (b) XPS of PS/CNC nanofibrous mats

Table 2 Surface oxygen content of PS/CNC nanofibrous mats

Code	Oxygen (at%)
PS	0.22
PS/CNC-1	1.37
PS/CNC-3	1.87
PS/CNC-5	2.46
PS/CNC-7	4.22

WXRD diffraction patterns of pure CNC and electrospun PS/CNC nanofibrous mats are shown in Fig.6. Data were smoothed over 40 adjacent points and were then normalized before plotting so that the main peaks had the same y-axis values for a direct comparison. For pure CNC, the typical peaks distributed at 2θ=16° and 22.5° were belonged to (101) and (002) crystal plane, respectively. Two typical diffraction peaks at 2θ = 19 and 22° for the electrospun PS nanofibrous mat are attributed to (110) and (220) crystal plane, respectively. For all PS/CNC nanofibrous mats, no new diffraction peaks were observed. However, with increased CNC content, the peak at 2θ=22° for nanofibrous mats was broadened and strengthened gradually, indicating that the peak of PS (220) crystal plane was overlapped with that of (002) crystal plane of CNC. With the addition of crystalline CNCs to the PS matrix, the (110) plane had little variation. The calculated CI values of PS/CNC nanofibrous mats were 22.0, 24.5, 25.8, and 27.2% for PS/CNC-1, 3, 5, and 7, respectively. Apparently, the CI values of electrospun nanofibrous mats increased with increasing CNC loading level, which was mainly due to the high-crystalline structure of CNC (CI=88%). Because when MCC was hydrolyzed to produce CNCs, non-crystalline region of MCC could be destroyed but crystalline region could be retained (Fig.1) [6], resulting in high crystalline degree of CNC. Furthermore, it is also indicated that the CI of nanofibers could be enhanced by reducing nanofiber diameters, ascribing that the smaller diameters could result in higher molecular orientation [35]. With high CNC content, therefore, the PS/CNC nanofibers electrospun could exhibit more ordered orientation because of their smaller diameters, leading to an increment of crystalline degree of PS/CNC nanofibers. Taken together, the CI of the electrospun PS/CNC nanofibers can be synergistically altered by CNC content and fiber diameter. The increased CI values for PS/CNC nanocomposites contributed to the mechanical property as discussed later in the paper.

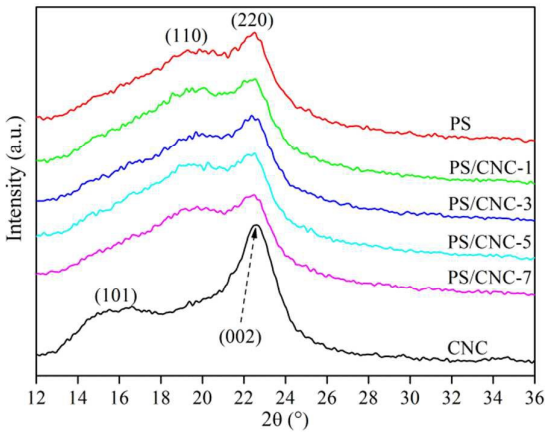

Fig.6. WXRD patterns of pure CNC and electrospun PS/CNC nanofibrous mats

3.4 Thermal Behavior of Nanofibrous Mats

Fig.7 shows the DSC curves of electrospun PS/CNC nanofibrous mats. In addition, Table 3 summarizes the temperature data obtained from thermal behavior tests. In Fig.7, it is shown that all the DSC curves exist single glass transition peak around 100℃, corresponding to the glass transition of PS (92℃ listed in Table 3). It also can be seen that with increasing CNC content in PS/CNC nanocomposite, the T_gs of PS/CNC nanocomposites were gradually elevated from 94 to 101℃, indicating a positive enhancement in modifying the T_g of PS. This thermal behavior can be explained by a combination of hydrogen bond crosslinking effect between CNCs [36] and mechanical percolation effect [37]. As CNCs were distributed both inside the nanofibers and on the surface of the nanofibers, the physical crosslinking between CNCs originated from hydrogen bond could be formed at single nanofiber and among nanofibers, thus resulting in a great increment for the thermal transformation temperature of nanofibers. Favier et al. [38] studied the mechanical percolation effect in nanocomposite films of cellulose whisker and poly(butyl acrylate-co-styrene). They found that adding cellulose crystals could drastically enhance properties of composites, even when the whisker weight fraction was only a few percent, and this behavior was driven mainly by the mechanical percolation properties of the cellulose network. In electrospun PS/CNC nanofibrous mats, the mechanical percolation effect between CNCs and polymers resulted from rigid interconnected network of CNCs could further reduce the polymer chains rotation around transformation temperature, namely increasing the glass transition temperature. With increasing CNC loading level, as a consequence, the combination effect of forming strong physical crosslinking network and mechanical percolation can be gradually enhanced, leading to the increased T_gs.

Fig.8 illustrates the effect of CNC on the thermal behavior of PS/CNC nanofibrous mats measured by TGA. In Fig.8(a), the TGA curve of CNCs showed a two-step thermal decomposition process with T_{onset} at 245.2℃ and 348.6℃, respectively, while the TGA thermogram of electrospun pure PS nanofibrous mats displayed typical single-step decomposition process with T_{onset} at 385.1℃. It can be observed that the two-step thermal decomposition trend of electrospun PS/CNC nanofibrous mats turned to be more obvious with increasing the addition of CNCs. However, although T_{onset} of PS/CNC nanocomposites decreased when increasing CNC content, the second thermal decomposition temperatures were all higher than that of electrospun PS fibrous mat. From Table 3, it is shown that when 7wt% CNCs were incorporated, the thermal decomposition temperature could be elevated to 421.4℃. In Fig.8(b), it is presented that the two-step decomposition of PS/CNC nanocomposites with 5 wt% and 7wt% CNCs was evidenced. It is also shown that the T_{max} of the electrospun nanofibrous mats shifted to the higher temperature from 416.2 to 426.4℃ with adding more CNCs. The improved thermal stability of PS/CNC nanofibrous mats is ascribed that CNCs could interconnect with each other during electrospinning to form rigid interconnected network, and also the CNCs could form mechanical percolation effect with PS. Furthermore, the surface $-SO_3H$ group of CNCs could be associated with each other to form physical crosslinking structure, which also increased the thermal stability. It is demonstrated that while the two-step decomposition characteristic of CNC could dominate the decomposition process, the homogeneously dispersed CNCs could provide significant enhancement to improve the thermal behavior.

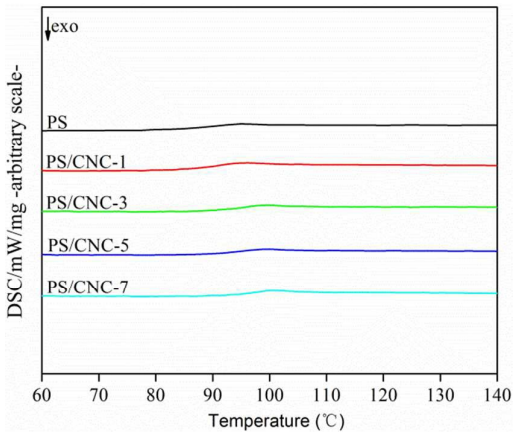

Fig.7. DSC curves of electrospun PS/CNC nonofibrous mats

Table 3 Thermal properties of electrospun nanofibrous mats

Code	T_g (℃)	T_{onset} (℃)[a]	T_{max} (℃)[a]
PS	92	—/385.1	—/416.2
CNC	—	245.2/348.6	281.7/—
PS/CNC-1	94	—/383.2	—/416.9
PS/CNC-3	96	279.1/392.7	287.9/419.5
PS/CNC-5	99	248.8/399.2	252.4/423.7
PS/CNC-7	101	220.6/405.4	236.1/426.4

[a] T_1/T_2 represented the temperatures in two-step thermal decomposition.

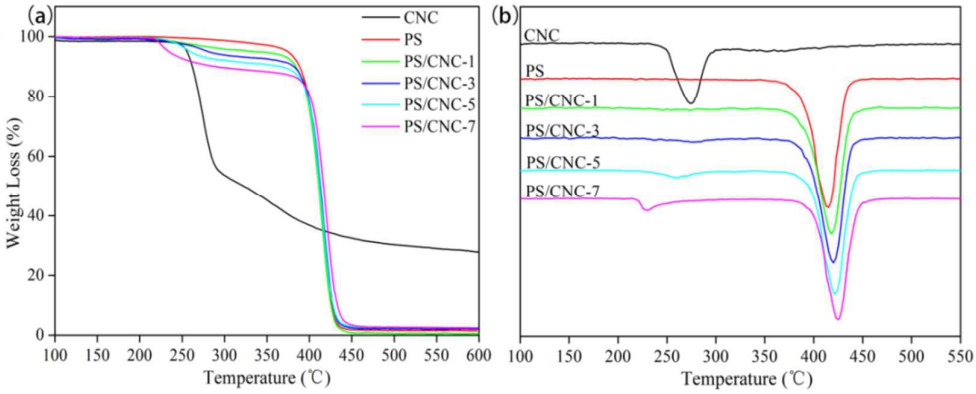

Fig.8. (a) TGA and (b) DTG results of CNCs and electrospun PS/CNC nonofibrous mats

3.5 Tensile properties of Nanofibrous Mats

Typical stress-strain curves of electrospun PS/CNC nanofibrous mats are presented in Fig.9(a). The maximum tensile stress (σ_{max}) and the elongation at break (ε_b) obtained from the curves are summarized in Fig.9(b) with data listed in Table 4. The tensile properties were significantly reinforced with increased CNC content in the PS matrix. The σ_{max} of PS/CNC nanofibrous mats at 7 wt% loading level was 0.4 MPa, which was increased by 170% compared to that of pure PS electrospun mat (0.15 MPa), indicating the significant reinforcement achieved from CNCs. Correspondingly, a decreasing trend was observed for the ε_b as the CNC content increased. This reinforcement effect was likely attributed to two main reasons. First, such superior mechanical properties could benefit from the mechanical percolation effect between PS chains and CNCs, and from the strong interactions between CNC themselves, both promoting the formation of rigid interconnected network structure to resist the tensile process [39-40]. Second, the high degree crystallinity of electrospun PS/CNC nanofibers could be responsive for the improved mechanical properties. Lim et al. [41] demonstrated that the densely packed nanofibers and fibrillary structures aligned themselves played an important role in enhancing the mechanical properties of nanofibers. It was suggested that the fibrillary structure having a high degree of crystallinity and molecular orientation could provide high resistance to axial tensile force. For the electrospun PS/CNC nanofibrous mats with low CNC content, the crystallinity degree of electrospun nanofibers was lower because of low CNC content, larger fiber

diameter and lack of ordered orientation. Furthermore, the rough surface of nanofibers with low CNC loadings can reduce the amount of closely packed nanofibers due to the large cracks when impacted [17]. Thus under certain stress, the incompact and low crystallinity degree nanofibers were soft to resist the stress, leading to a smaller σ_{max} but larger ε_b. For the nanofibers with high CNC content, however, the nanofibers featuring higher crystallinity degree and smooth surface could be closely packed with each other than that of the rough ones and be aligned to orderly pattern. When tested, the impacted fibers can afford enough resistance to temporarily balance with the stress, showing superior strength (large σ_{max}) but little ductility (small ε_b).

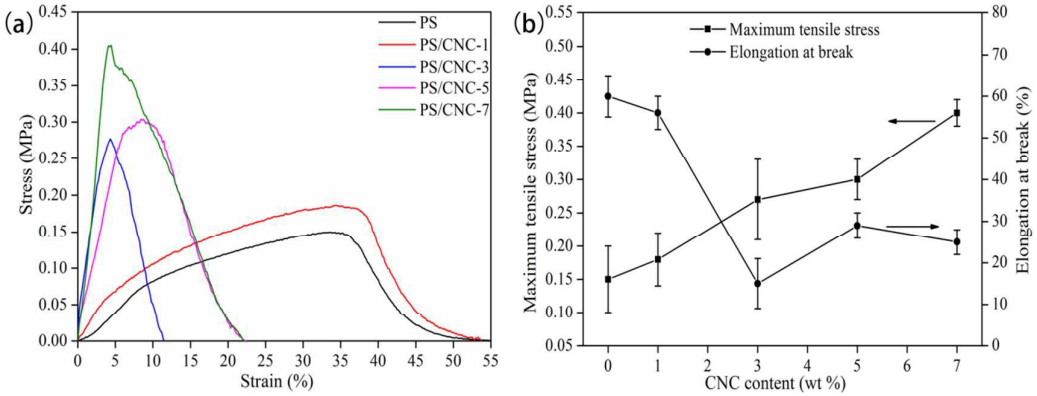

Fig.9. (a) Stress-strain curves of electrospun PS/CNC nanofibrous mats (b) Tensile properties of electrospun PS/CNC nanocomposite mats as a function of CNC contents

Table 4 Tensile properties of electrospun nanofibrous mats

Code	Thickness (mm)	σ_{max} (MPa)	ε_b (%)
PS	0.11±0.02	0.15±0.05	60±5
PS/CNC-1	0.09±0.01	0.18±0.04	56±4
PS/CNC-3	0.08±0.03	0.27±0.06	15±6
PS/CNC-5	0.09±0.01	0.30±0.03	29±3
PS/CNC-7	0.09±0.02	0.40±0.02	25±3

3.6 Wettability of Nanofibrous Mats

The CA values of electrospun PS/CNC nanocomposites are displayed in Fig.9. It is observed that the PS nanofibrous mat had a CA value of 120°, whereas the CA was significantly elevated to 138° after adding 1 wt% CNCs. With further increased addition of CNCs from 3 to 7 wt%, the CA values were somehow levelled off. The proposed mechanism to tune the hydrophilic-hydrophobic property of electrospun PS/CNC nanofibrous mats is a dynamic combination of the spatial arrangement of nanofibers [42], chemical properties of nanofibers [7], and the surface structure of nanofibrous mats [43]. The ordered spatial arrangement of nanofibers is a positive effect to enhance the hydrophobicity. It is ascribed that when nanofibers were orderly packed, the nanofibers could be arranged as ordered criss-cross morphology, with which the water drops could be effectively squeezed out. With increasing the addition of CNCs, the aligned structure of nanofibers could be achieved as discussed early, then producing hydrophobic property. It has been well known that the hydrophobicity of nanofiber surface can also be controllably tuned by surface chemical composition. In this contribution, the addition of NSM in PS/CNC spinning solutions could form water-in-oil suspension in which the hydrophilic -OH of CNCs was protected by the hydrophobic moiety of NSM. Thus the hydrophobically protected CNCs either located on the surface of PS nanofibers, or incorporated into PS nanofibers could provide water-fearing effect on nanofiber surface. This is attributed that combining the formed CNCs interconnected network, the long alkane chains of NSM could stretch to cover more surface area of nanofibers under rapid electrospinning process. However, the surface roughness of electrospun nanofibrous mats also plays a crucial role in determining the hydrophobicity because more air can be trapped with rough surface, which is beneficial for hydrophobicity since the water CA of air is considered to be 180° [44]. With adding more CNCs into PS matrix, the surface structure of electrospun PS/CNC nanofibers was turned to be smooth, which provided negative effect to surface hydrophobicity of nanofibers. Thus the advantages gained from adding CNCs by electrospinning in terms of a potential for

elevating surface hydrophobicity were partially offset by less nanofiber surface roughness, resulting in a downward but leveling-off trend with high CNC loadings.

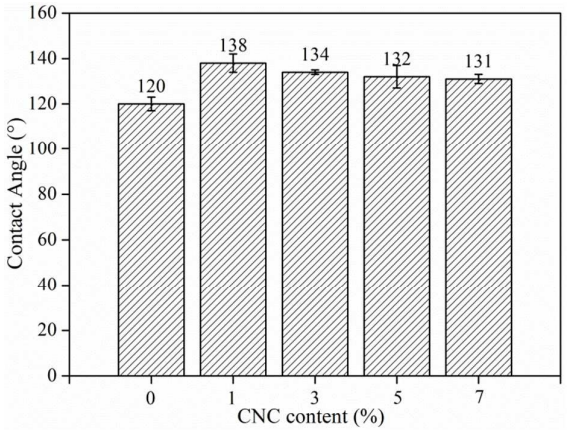

Fig.10. CA values of electrospun neat PS and PS/CNC nanocomposites

4 Conclusions

Nanofibrous composites of PS reinforced with CNCs were successfully produced through electrospinning process. Surfactant NSM was added to achieve the desired homogeneous dispersion of CNCs in PS matrix. Fine nonwoven nanofibrous mats with homogeneous nanofiber diameter and smooth surface were obtained, showing enhanced crystallinity as a result of the addition of CNCs to the PS polymer matrix and the aligned nanofiber molecular orientation. The additive of CNCs was physically mixed with PS and probably distributed on electrospun nanofiber surface according to FTIR and XPS. The thermal properties of PS/CNC nanocomposites were significantly improved, ascribing to the limited polymer chains rotation induced by formed interconnected network of CNCs and the mechanical percolation effect of PS and CNCs. The tensile strength of PS/CNC nanofibrous mats with 7wt% CNCs was elevated to 0.4 MPa and increased by 170% compared with electrospun pure PS nanofiber, which was attributed to the high crystallinity and percolation effect to resist the tensile force. A significant enhancement in hydrophobicity of electrospun PS/CNC nanofibrous mats was achieved due to the synergistic effect of nanofiber morphology and surface chemical composition. Overall, these outcomes demonstrate that electrospinning simple blending of hydrophobic PS and hydrophilic CNCs can manufacture PS/CNC nanocomposite materials with superior performances.

Acknowledgements

This work was financially supported by the State Forestry Bureau 948 project (Grant No. 2013-4-11), the National Natural Science Foundation of China (Gant No. 31470580), and the Fundamental Research Funds for the Central Universities (Grant No. 2572014AB14).

References

[1] J. P. F. Lagerwall, C. Schutz, M. Salajkova, J. H. Noh, J. H. Park, G. Scalia, L. Bergstrom. Cellulose nanocrystal-based materials: from liquid crystal self-assembly and glass formation to multifunctional thin films. *NPG Asia Mater.*, 2014, 6: 1-12.

[2] A. Bishopp, M. J. Bennett. Seeing the wood and the trees. *Nature*, 2015, 517: 558-559.

[3] J. L. W. Morgan, J. Strumillo, J. Zimmer. Crystallographic snapshot of cellulose synthesis and membrane translocation. *Nature*, 2013, 493: 181-186.

[4] H. Yan, W. X. Zhang, X. W. Kan, L. Dong, Z. W. Jiang, H. J. Li, H. Yang, R. S. Cheng. Sorption of methylene blue by carboxymethyl cellulose and reuse process in a secondary sorption. *Colloid. Surface. A*, 2011, 380: 143-151.

[5] K. A. Iyer, G. T. Schueneman, J. M. Torkelson. Cellulose nanocrystal/polyolefin biocomposites prepared by solid-state shear pulverization: Superior dispersion leading to synergistic property enhancements. *Polymer*, 2015, 56: 464-475.

[6] G. P. Han, S. Q. Huan, J. Q. Han, Z Zhang, Q. L. Wu. Effect of acid hydrolysis conditions on the properties of cellulose nanoparticle-reinforced polymethylmethacrylate composites. *Materials*, 2014, 7: 16-29.

[7] P. Stenstad, M. Andresen, B. S. Tanem, P. Stenius. Chemical surface modifications of microfibrillated cellulose. *Cellulose*, 2008, 15: 35-45.

[8] W. Li, J. Q. Yue, S. X. Liu. Preparation of nanocrystalline cellulose via ultrasound and its reinforcement capability for poly(vinyl alcohol) composites. *Ultrason. Sonochem.*, 2012, 19: 479-485.

[9] H. Kargarzadeh, R. M. Sheltami, I. Ahmad, I. Abdullah, A. Dufresne. Cellulose nanocrystal: A promising toughening agent for unsaturated polyester nanocomposite. *Polymer*, 2015, 56: 346-357

[10] D. Klemm, F. Kramer, S. Moritz, T. Lindstrom, M. Ankerfors, D. Gray, A. Dorris. Nanocelluloses: A new family of nature-based materials. *Angew. Chem. Int. Ed.*, 2011, 50, 5438-5466.

[11] E. A. Appel, M. W. Tibbitt, M. J. Webber, B. A. Mattix, O. Veiseh, R. Langer. Self-assembled hydrogels utilizing polymer-nanoparticle interactions. *Nat. Commun.*, 2015, DOI: 10.1038/ncomms7295.

[12] J. Yang, C. R. Han, F. Xu, R. C. Sun. Simple approach to reinforce hydrogels with cellulose nanocrystals. *Nanoscale*, 2014, 6: 5934-5943.

[13] Y. Habibi, L. A. Lucia, O. J. Rojas. Cellulose nanocrystals: Chemistry, self-assembly, and applications. *Chem. Rev.*, 2010, 110: 3479-3500.

[14] E. Celia, T. Darmanin, E. T. de Givenchy, S. Amigoni, F. Guittard. Recent advances in designing superhydrophobic surfaces. *J. Colloid. Interf. Sci.*, 2013, 402: 1-18.

[15] K. A. Krishnan, R. Anjana, K. E. George. Effect of alkali-resistant glass fiber on polypropylene/polystyrene blends: Modeling and characterization. *Polym. Composite.*, 2014, DOI: 10.1002/pc.23193

[16] L. Bai, J. Y. Gu, S. Q. Huan, Z. G. Li. Aqueous poly(vinyl acetate)-based core/shell emulsion: synthesis, morphology, properties and application. *RSC Adv.*, 2014, 4: 27363-27380.

[17] S. Q. Huan, G. X. Liu, G. P. Han, W. L. Cheng, Z. Y. Fu, Q. L. Wu, Q. W. Wang. Effect of experimental parameters on morphological, mechanical and hydrophobic properties of electrospun polystyrene fibers. *Materials*, 2015, 8: 2718-2734.

[18] G. Ahmetli, A. Cerit. Effects of functional groups on the thermal properties of modified polystyrene. *J. Appl. Polym. Sci.*, 2007, 104: 2549-2553.

[19] M. Worzakowska. Thermal and mechanical properties of polystyrene modified with esters derivatives of 3-phenylprop-2-en-1-ol. *J. Therm. Anal. Calorim.*, 2015, DOI 10.1007/s10973-015-4547-7

[20] N. Lin, A. Dufresne. Nanocellulose in biomedicine: Current status and future Prospect. *Eur. Polym. J.*, 2014, 59: 302-325.

[21] N. Lin, A. Dufresne. Supramolecular hydrogels from in situ host guest inclusion between chemically modified cellulose nanocrystals and cyclodextrin. *Biomacromolecules*, 2013, 14:871-880.

[22] M. Bercea, P. Navard. Shear dynamics of aqueous suspension of cellulose whiskers. *Macromolecules*, 2000, 33, 6011-6016.

[23] R. Menini, M. Farzaneh. Production of superhydrophobic polymer fibers with embedded particles using the electrospinning technique. *Polym. Int.*, 2008, 57: 77-84.

[24] Y. L. Yoon, H. S. Moon, W. S. Lyoo, T. S. Lee, W. H. Park. Superhydrophobicity of cellulose triacetate fibrous mats produced by electrospinning and plasma treatment. *J. Colloid. Interf. Sci.*, 2008, 320: 91-95.

[25] A. Greiner, J. H. Wendorff. Electrospinning: A fascinating method for the preparation of ultrathin fibers. *Angew. Chem. Int. Ed.*, 2007, 46: 5670-5703.

[26] D. He, B. Hu, Q. F. Yao, K. Wang, S. H. Yu. Large-scale synthesis of flexible free-standing SERS substrates with high sensitivity: electrospun PVA nanofibers embedded with controlled alignment of silver nanoparticles. *ACS Nano*, 2009, 3: 3993-4002.

[27] Q. F. Shi, C. J. Zhou, Y. Y. Yue, W. H. Guo, Y. Q. Wu, Q. L. Wu. Mechanical properties and in vitro degradation of electrospun bio-nanocomposite mats from PLA and cellulose nanocrystals. *Carbohyd. Polym.*, 2012, 90: 301-308.

[28] M. S. Peresin, Y. Habibi, J. O. Zoppe, J. J. Pawlak, O. J. Rojas. Nanofiber composites of polyvinyl alcohol and cellulose nanocrystals: Manufacture and characterization. *Biomacromolecules*, 2010, 11: 674-681.

[29] C. J. Zhou, R. Chu, R. Wu, Q. L. Wu. Electrospun polyethylene oxide/cellulose nanocrystal composite nanofibrous mats with homogeneous and heterogeneous microstructures. *Biomacromolecules*, 2011, 12: 2617-2625.

[30] O. J. Rojas, G. A. Montero, Y. Habibi. Electrospun nanocomposites from polystyrene loaded with cellulose

nanowhiskers. *J. Appl. Polym. Sci.*, 2009, 113, 927-935.

[31] C. J. Zhou, Q. L. Wu, Q. G. Zhang. Dynamic rheology studies of in situ polymerization process of polyacrylamide-cellulose nanocrystal composite hydrogels. *Colloid Polym. Sci.*, 2011, 289: 247-255.

[32] T. Lin, H. X. Wang, H. M. Wang, W. G. X. The charge effect of cationic surfactants on the elimination of fibers bead in the electrospinning of polystyrene. *Nanotechnology*, 2004, 15: 1375-1381.

[33] D. Li, Y. N. Xia. Electrospinning of nanofibers: Reinventing the wheel?. *Adv. Mater.*, 2004, 16: 1151-1170.

[34] H. Kargarzadeh, I. Ahmad, I. Abdullah, A. Dufresne, S. Y. Zainudin, R. M. Sheltami. Effects of hydrolysis conditions on the morphology, crystallinity, and thermalstability of cellulose nanocrystals extracted from kenafbast fibers. *Cellulose*, 2012, 19:855-866.

[35] S. C. Wong, A. Baji, S. W. Leng. Effect of fiber diameter on tensile properties of electrospun poly(3-caprolactone). *Polymer*, 2008, 49: 4713-4722.

[36] V. Favier, H. Chanzy, J. Y. Cavaille. Polymer nanocomposites reinforced by cellulose whiskers. *Macromolecules*, 1995, 28:6365-6367.

[37] A. Kaboorani, B. Riedl, P. Blanchet, M. Fellin, O. Hosseinaei, S. Wang. Nanocrystalline cellulose (NCC): A renewable nano-material for polyvinyl acetate (PVA) adhesive. *Eur. Polym. J.*, 2012, 48: 1829-1837.

[38] V. Favier, G. R. Canova, S. C. Shrivastava, J. Y. Cavaille. Mechanical percolation in cellulose whisker nanocomposites. *Polym. Eng. Sci.*, 1997, 37, 1732-1739.

[39] V. Favier, G. R. Canova, J. Y. Cavaillé, H. Chanzy, A. Dufresne, C. Gauthier. Nanocomposite materials from latex and cellulose whiskers. *Polym. Adv. Tech.*, 1995, 6: 351-355.

[40] V. Favier, H. Chanzy, J. Y. Cavaille. Polymer nanocomposites reinforced by cellulose whiskers. *Macromolecules*, 1996, 28: 6365-6367.

[41] C. T. Lim, E. P. S. Tan, S. Y. Ng. Effects of crystalline morphology on the tensile properties of electrospun polymer nanofibers. *Appl. Phys. Lett.*, 2008, 92: 141908-1-3.

[42] L. Feng, S. H. Li, H. J. Li, J. Zhai, Y. L. Song, L. Jiang, D. B. Zhu. Super-hydrophobic surface of aligned polyacrylonitrile nanofibers. *Angew. Chem. Int. Ed.*, 2002, 41: 1221-1223.

[43] L. Feng, S. H. Li, Y. S. Li, H. J. Li, L. J. Zhang, J. Zhai, Y. L. Song, B. Q. Liu, L. Jiang, D. B. Zhu. Super-hydrophobic surface: from natural to artificial. *Adv. Mater.*, 2002, 14: 1857-1860.

[44] A. B. D. Cassie, S. Baxter. Wettability of porous surfaces. *Trans. Faraday Soc.*, 1944, 40: 546-551.